Design and simulation of a multichannel sensing system for liquid refractometry based on integrated photonics

A.G. Zakoyan [1], G.S. Voronkov [1], V.S. Lyubopytov [1], A. K. Sultanov [1], E.P. Grakhova [1], R.V. Kutluyarov [1]
[1] Ufa University of Science and Technology, 450076, Ufa, Russia, Z. Validi str., 32

Abstract

The paper proposes a new architecture for the photonic laboratory-on-a-chip sensing systems, where multiple sensors based on microring resonators (MRR) are fed by a MRR with low quality factor, working as a spectrum shaper. This architecture enables simultaneous intensity scanning of at least four MRR-based sensors on the silicon-on-insulator platform. We evaluated numerically the system's sensitivity for various schemes of connecting the sensors and the spectrum shaper. The sensor's sensitivity was 110 nm/RIU. The sensing system configuration largely determines its sensitivity, which reaches 1980 dB/RIU. The considered architecture may be useful for implementing fully integrated optical lab-on-a-chip structures, as well as distributed multichannel sensing systems.

Keywords: lab-on-a-chip, sensing system, integrated photonics, silicon-on-insulator, ring resonators.

Citation: Zakoyan AG, Voronkov GS, Lyubopytov VS, Sultanov AK, Grakhova EP, Kutluyarov RV. Design and simulation of a multichannel sensing system for liquid refractometry based on integrated photonics. Computer Optics 2023; 47(6): 884-894. DOI: 10.18287/2412-6179-CO-1268.

Acknowledgments: The research was supported by the Ministry of Science and Higher Education of the Russian Federation: state assignment for USATU, agreement № 075-03-2021-014 dated 29.09.2021 (FEUE-2021-0013).

Introduction

Today, lab-on-a-chip systems are one of the fastest-growing areas in applied photonics and biophotonics. Measurements in such systems should be carried out for several sensors that record specific changes in the environment, for example, in the composition of a liquid analyte. Critical requirements for such systems are high energy and cost efficiency, small footprint, and low weight. Thus, it is advantageous to implement lab-on-a-chip systems using integrated photonics technologies.

Widely used integrated photonic schemes for detecting changes in the physical properties of an analyte include: waveguide Bragg gratings (WBG) [1], waveguide Mach–Zehnder interferometers (MZI) [2, 3], microring (MRR), microdisk (MDR) or subwavelength grating microring resonators [4 – 7]. Label-free sensors based on microring resonators (MRRs) are among the most frequently studied photonic integrated circuit (PIC) designs for refractive analysis of the environment (liquids, gases) [8 – 11]. MRR in sensing applications is a compact, efficient, and high-accuracy solution. The compactness and accuracy make this type of sensor suitable, among other things, for creating fully integrated lab-on-a-chip optical systems. Currently, the main tasks in developing MRR-based sensors are to increase their sensitivity and quality factor, as well as methods for their interrogation. Three methods of scanning liquid sensors based on MRR are usually considered: interrogation by intensity [11, 12], frequency [13], and time [14].

Traditional interrogation systems based on tunable lasers or diffraction systems are unsuitable for full system implementation based on photonic integrated circuits. In turn, the classical architecture of the integrated sensing system "sensor – interrogator" does not meet the requirements for the simultaneous interrogation of several sensors. The principle of lab-on-a-chip systems dictates creating a sensing system that allows to simultaneously register changes in environmental parameters with several sensors. The examples mentioned above do not allow satisfying this requirement using only onecommon interrogating element for all sensors. Intensity-based interrogation in an integrated design requires each sensor to be connected in series to another MRR interrogator. At the same time, cascades of serially connected MRRs are actively used in conjunction with the Vernier effect scale to increase the sensitivity and quality factor of sensors [15, 16].

Sensor array interrogation is frequently used in fiber Bragg grating (FBG) scanning. In this case, it is possible to separate the information received from the sensors by frequency (wavelength) and time. With frequency division in the interrogation scheme, an arrayed waveguide grating (AWG) can be used to separate scanning channels [17] and provide wavelength division multiplexing (WDM) [18]. In the time division scheme [19], combinations of different techniques are often used, including, for example, the use of WDM [20], CDM-WDM (code-division multiplexing-wavelength-division multiplexing) [21], or the wavelength-to-time mapping method (or temporal self-imaging effect) [23]. The most importantadvantage of these methods is the ability to interrogate an array of tens and hundreds of sensors. However, implementing such schemes on a PIC is difficult or impossible.

Our proposed method combines intensity interrogation and cascading of several MRRs, which allows reducing the number of elements in the scanning scheme since we use only one element (the spectrum shaper) to register the parameters of several sensors.

To our knowledge, there have been no studies of PIC-based intensity interrogation of an optical sensors array using only one scanning element. This paper presents a scheme for the simultaneous interrogation of several refractometric MRR-based liquid sensors using a single MRR-based spectrum envelope shaper. Also, we analyzed different methods for detecting sensor indicators using the through and drop ports of the spectrum shaper MRR.

1. System structure and operation principle

As mentioned above, the "sensor–interrogator" structure, built on two MRRs (high-Q sensor and low-Q interrogator, Fig. 1*a* [8]), is suitable for creating a fully integrated sensing system, but is not applicable for simultaneous interrogation of several sensors. Here we employ the traditionally used designation of the MRR ports, [22] describes their functionality in detail. The described scheme provides converting the change in the resonant wavelength of the sensor into the light intensity and then into the photocurrent of photodiodes (PD) due to the use of a quasi-linear section of the interrogator transmission spectrum. Fig. 1*b* [11] shows this operation principle for the refractometry sensing system with analyte refractive index (RI) changing from RI1 to RI5. However, adding an additional sensor before the interrogator will mix the impact results from different sensors, and the sensing system will be inoperable. Therefore, we propose to invert the system structure in order to interrogate several sensors and use a low-Q MRR as a broadband interrogating signal spectrum shaper (Fig. 2). In this case, the transmission spectrum of the shaper MRR is the same as for an interrogator MRR (Fig. 1*b*). The sensor input signal intensity varies according to the shaper transmission spectrum. One can get the input signals for several sensors by dividing the shaper output signal using integrated optical splitters. Fig. 3 shows an example of such a structure for interrogating four sensors. Essentially, the number of sensors depends on the circuit attenuation, the sensitivity and type of the photodiodes used, and the power of the broadband source. The spectrum of the broadband signal at the spectrum shaper output is a domed function. Thus, the value of the photocurrent on each photodiode is determined by the mutual arrangement of the transmission spectra of the sensors and the spectrum shaper. We considerth is aspect in more detail in Section 4.

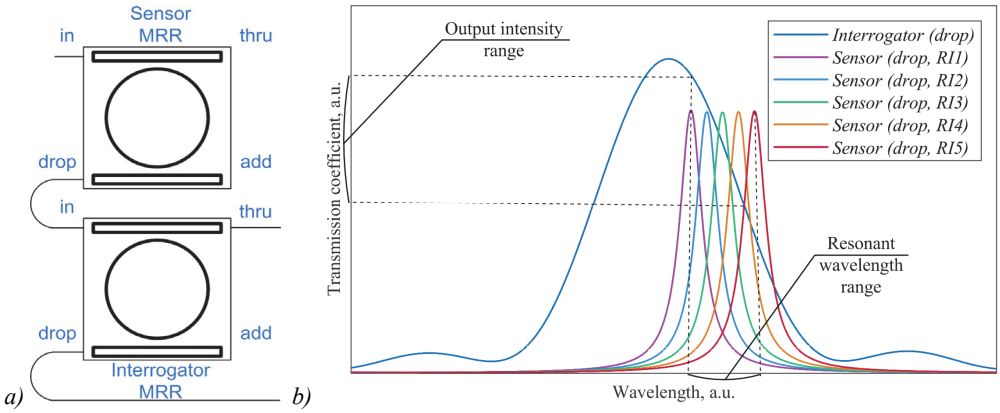

Fig. 1. "Sensor – interrogator" structure (a) and operation principle (b)

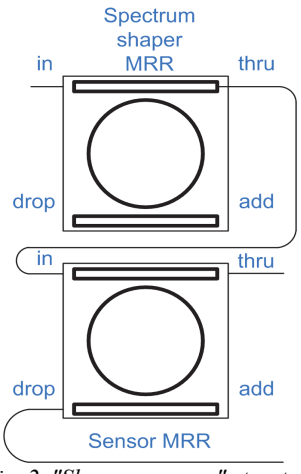

Fig. 2. "Shaper – sensor" structure

This work analyzes two different spectrum shapers with different transmission spectra and the wavelength bands of the quasi-linear section. This causes some features in the sensor's modeling (see Section 2), since it is necessary to simulate its operationin the two corresponding wavelength bands. Designs the of the spectrum shaper and their transfer characteristics are described in more detail in Section 4.

2. MRR sensor design and parameters

The developed label-free sensor model for liquid analysis based on a racetrack MRR on the silicon-on-insulator (SOI) platform was simulated using Ansys Lumerical software. Characteristics of the materials for simulation are taken from [24]. Wedesigned the MRR for the standard SOI process with the Si layer height

0.22 μ*m*, and the waveguide width 0.4 μ*m*. Fig. 4 shows the sensor MRR topology and dimensions. The frequency response of the MRR was calculated using the FDTD (Finite Difference Time Domain) method in Ansys Lumerical software with the following parameters: simulation time – 7000 fs, mesh accuracy – 3, minimum mesh step – 0.25 nm, monitor frequency points – 7000. The calculation was carried out for the TE-mode.

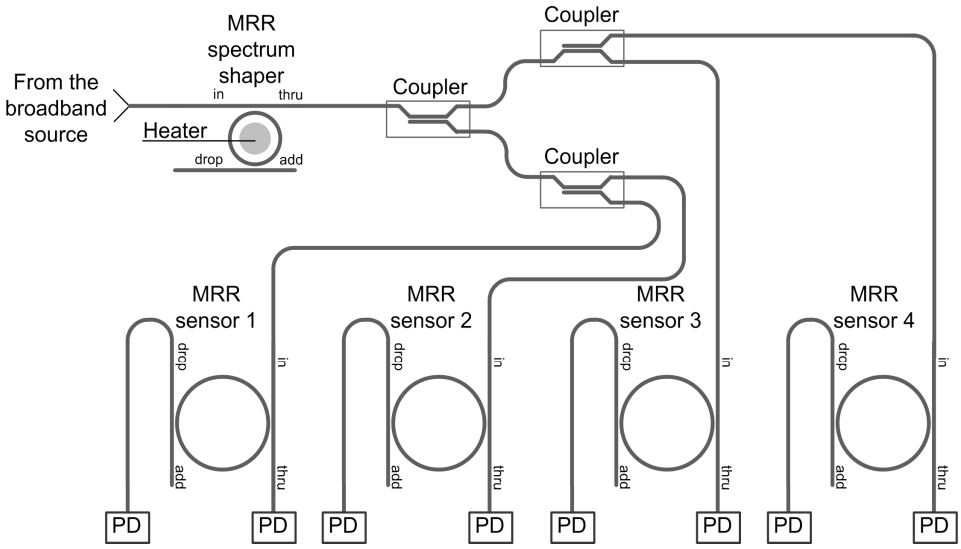

Fig. 3. Multichannel sensing system structure (not for scale); 'in', 'thru', 'add', 'drop' are the MRR's input, through, add and drop ports, respectively; PD - photodiode

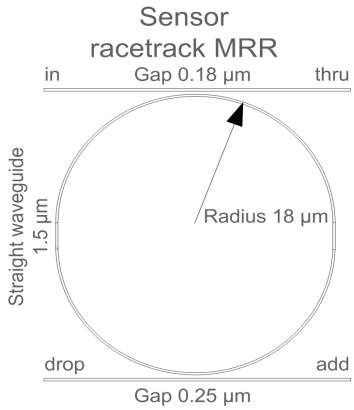

Fig. 4. Sensor racetrack MRR topology

The dispersion, loss, effective RI, and group RI of the waveguide were defined using the Finite Difference Eigenmode Solver in Lumerical MODE. The MRR calculation method was employed as presented in [25, 26].

Transfer functions of MRR at the output of through and drop ports are determined by the frequency response [27]:

$$T_{thru} = \left|\frac{E_{thru}}{E_{in}}\right|^2 = \left|\frac{r_1 - r_2 \cdot e^{-\alpha L/2} \cdot e^{i\beta L}}{1 - r_1 r_2 \cdot e^{-\alpha L/2} \cdot e^{i\beta L}}\right|^2, \quad (1)$$

$$T_{drop} = \left|\frac{E_{drop}}{E_{in}}\right|^2 = \left|\frac{-\kappa_2 \kappa_2 \cdot e^{-\alpha L/4} \cdot e^{i\beta L}}{1 - r_1 r_2 \cdot e^{-\alpha L/2} \cdot e^{i\beta L}}\right|^2, \quad (2)$$

where E_{thru}, E_{drop}, E_{in} are mode amplitudes in the through, drop, and input MRR ports; α – the loss coefficient of the ring waveguide; $\beta = 2\pi n_{eff}/\lambda$ – propagation constant; λ – wavelength; n_{eff} – effective RI; κ_1, κ_2 – coupling coefficients at the top and bottom couplers of the ring resonator; r_1, r_2 – transmission coefficients in the in-though and add-drop waveguides; $L = 2\pi R + 2L_s$ – circumference of the racetrack, R – radius of the ring, L_s – the length of the straight waveguide in the racetrack.

Fig. 5 shows the transmission spectrum at the through and drop ports of the designed sensor MRR. Its parameters were calculated for critical coupling condition in the ring [27, 28]. The gap value for the add-drop waveguide is larger than that for the input waveguide in order to reduce the coupling coefficient κ_2, which leads to narrowing the sensor FWHM (full width at half maximum, or 3 dB bandwidth $2\delta\lambda$ of the resonance line shape):

$$FWHM = 2\delta\lambda = \frac{\kappa_1 \kappa_2 \lambda_{res}^2}{\pi n_{eff} L}, \quad (3)$$

where λ_{res} – MRR resonant wavelength ($\lambda_{res} = 2\pi n_{eff} R/m$, m – the resonance number, n_{eff} – effective refractive index (RI). Tab. 1 shows calculated MRR sensor parameters.

Tab. 1. Sensor MRR parameters

Parameter	n_{eff}	n_g	κ_1,κ_2	Q	FSR	FWHM
Value	2.2	4.56	0.331, 0.215	7359	4.67 nm	0.21 nm

As will be described below, reducing the sensor's FWHM is necessary primarily to match its response with the response of the spectrum shaper MRR. It also increases the quality factor Q, free spectrum range (FSR), and sensitivity S of the sensing system:

$$Q = \frac{\lambda_{res}}{FWHM}, \quad (4)$$

$$FSR = \frac{\lambda^2}{n_g L}. \quad (5)$$

The actual relationship between FWHM of the sensors and the shaper MRR needs to be determined for specific application scenarios and sensors resonant wavelength range.

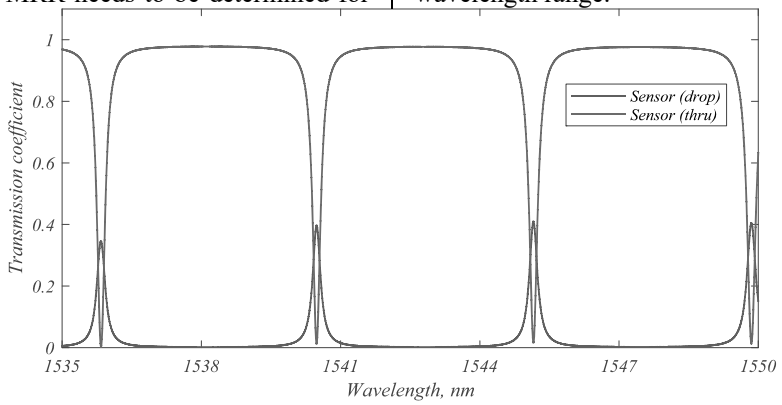

Fig. 5. Transmission spectra at the through and drop ports of the sensor MRR

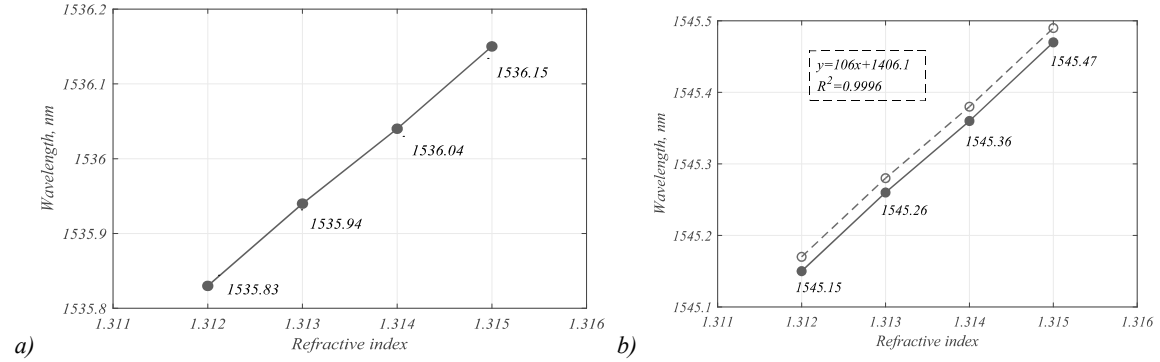

Fig. 6. (a) Relation between RI and the resonance shift in the first band; (b) Relation between RI and the resonance shift in the second band, compared with the linear approximation

The principle of operation of MRR-based liquid sensors is as follows: when the analyte is on the surface of the resonator, and the analyte RI changes (caused by a change in some liquid parameter), the effective RI of the sensor waveguides changes, which leads to a shift in the resonant wavelengths in the MRR transmission spectrum. Fig. 8 and 8 show the shift of sensor resonant wavelengths in the two considered wavelength bands as the effective RI of the analyte changes. From the results obtained, we determined that the sensor sensitivity *S* was:

$$S = \frac{\Delta\lambda}{\Delta n} = 110\ nm / RIU. \quad (6)$$

The minimum detectable change in the RI defines the limit of detection (LoD), which depends on the minimum detectable resonant wavelength shift [29]:

$$LoD(n) = \frac{\lambda_{res}}{S \cdot Q} = 1.98 \cdot 10^{-3} RIU. \quad (7)$$

To evaluate the linearity of the measuring characteristic, we additionally introduced the coefficient of non-linearity *D*, defined as:

$$D = \frac{\delta}{sm}, \quad (8)$$

where *sm* is the slope of the curve, and δ is the deviation relative to a linear function. The middle *D* only for the sensor MRR is about $1.98 \cdot 10^{-4}$ RIU.

3. MRR-based spectrum shaper

The proposed method of simultaneous intensity scanning of parallel-connected sensors implies the presence of an initial signal spectrum envelope. This envelope will change its shape at the circuit output depending on the sensor characteristics. Such a spectrum shaper can be implemented also based on a MRR.

Setting the shaper MRR parameters depends on the FWHM, FSR, and sensitivity of the sensors. These parameters must be coordinated so that the resonances of the sensor fall to the linear section of the spectral characteristics of the spectrum shaper, and the sensitivity determines the maximum number of sensors that can be interrogated simultaneously by this method. It is possible to solve the problem of adjusting the transmission spectra of the shaper and sensors by adding a thermo-optical phase-shifting element to the circuit.

The paper analyzes two interrogating schemes with two different MRR-based spectrum shapers. We defined their characteristics so that we could consider them in operation with the same sensors. Fig. 7 shows their layouts with geometric parameters. Therefore, Fig. 8 shows two ranges of sensor resonant wavelengths. The first version (MRR1) has the following characteristics: the radius is 10 μ*m*, the gap is 0.1 μ*m*, and the waveguide height and width are 0.22 and 0.4 μ*m*, respectively. The second version (MRR2) differs from the first one in small racetrack sections (straight

waveguides) 0.5 μ*m* long. Fig. 8 shows the spectral characteristics of the two shaper MRRs.

4. Overall sensing system simulation

To optimize the configuration of the interrogation scheme, we analyzed several system implementation options, differing in the shaped spectrum (using the shaper MRR's through or drop port, respectively) and the method of detecting the resulting characteristics.

It is necessary to ensure the fulfillment of the following condition to improve the quality of the sensing system: the resonant wavelengths of the sensors and the shaper are close to each other in the wavelength range used for the operation of the sensingsystem and are significantly different in the rest of the wavelength range of the broadband source. In practice, it is reasonable to select (design) a broadband source in such a way that its bandwidth slightly exceeds half the FWHM of the shaper, and thecentral wavelength corresponds to the middle of the monotonic section of the shaper transmission spectrum used to convert the sensor output wavelength into intensity.

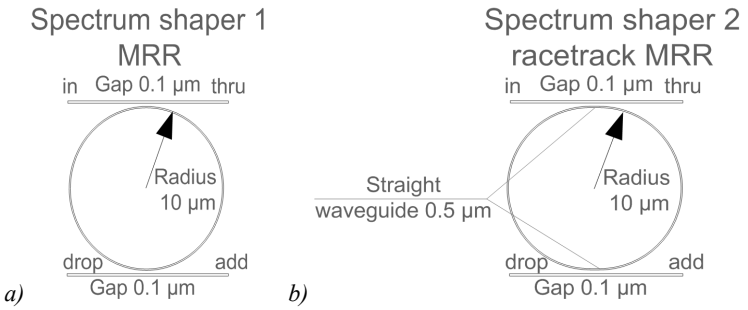

Fig. 7. Spectrum shaper MRR1 (a) and MRR2 (b) topologies

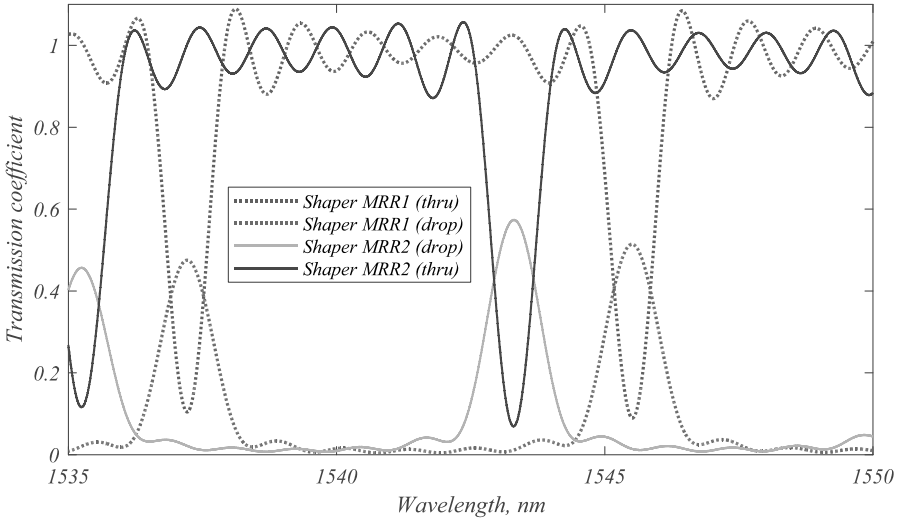

Fig. 8. Transmission spectra at the through and drop ports of the two considered types of the MRR shaper

We performed the simulations according to Fig. 3 using an optical network analyzer (ONA), which is a Lumerical Interconnect library element, as a broadband source. A 5 dBm output signal with a 10 nm bandwidth enters the input ('in') port ofthe envelope shaper MRR, from which, via a through or drop port, it enters the stage of splitters with a division factor of 0.5, which feed all the sensors. Photodetectors are connected to the sensors' through and drop ports and record the output power.

We estimated the overall sensing system sensitivity as a ratio of the change in the photodiode output power level ΔP_{pd} (measured in decibels) to the RI change that caused this change ΔRI:

$$S_m = \frac{\Delta P_{pd}}{\Delta RI} = \frac{P_{max} - P_{min}}{n_{max} - n_{min}}, [dB / RIU], \quad (9)$$

where P_{max} and P_{min} are the maximum and minimum values of output power, respectively, and n_{max} and n_{min} are the maximum and minimum values of the analyte RI.

We compared several sensing system architectures using S_m. In the first variant, we used the shaper's through port as a source for the sensor interrogation. We used the shaper's drop port in the second variant for this purpose. In both cases, we analyzed the sensors' through- and drop-ports power and the relative power. The relative power level P estimation makes it possible to eliminate the influence of instabilities (fluctuations) in the broadband source output power [11]. Its calculation is made for the drop port relative to the total output power:

$$P = \log\left(\frac{P_{drop}}{P_{drop} + P_{thru}}\right). \quad (10)$$

4.1. Using the shaper's through port as a signal source

The shaped spectrum from the through port of the MRR is fed through the splitters to the input of each sensor, as shown in Fig. 3. Fig. 9*a* and 9*b* show the spectral characteristics at the through ports of the sensors, showing the result of the interaction of two spectra for the scheme of operation with the shaper MRR1 and MRR2, respectively; Fig. 10*a* and 10*b* show the dependencies of the recorded power at the through ports of the sensors on the change in the liquid RI and the corresponding linear approximations. The calculated using (9) sensitivity for the two schemes is $S_{m1}=93.3$ dB/RIU and $S_{m2}=16.67$ dB/RIU.

We also analyzed the coefficient of non-linearity D using equation (8) for the whole sensing system; it equals $1.13\cdot10^{-4}$ RIU for the first scheme, and $1.47\cdot10^{-4}$ RIU for the second one.

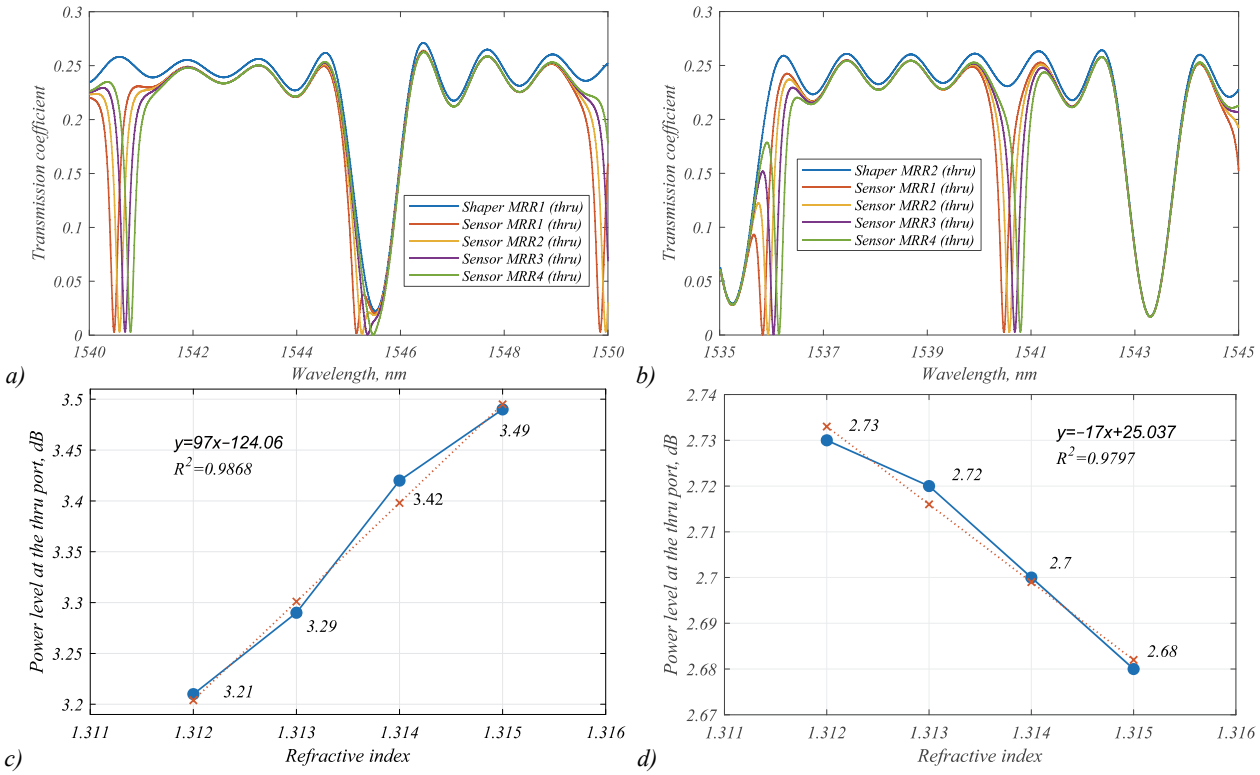

Fig. 9. Transmission spectra at the sensors' through ports depending on the spectrum shape coming from the through port of the shaper MRR (a) for the scanning circuit with MRR1, and (b) for the scanning circuit with MRR2; dependence of the received power on the through ports of the sensors on the change in the liquid RI and the linear approximation (c) for the scanning circuit with MRR1, and (d) for the scanning circuit with MRR2

Fig. 10*a* and 10*b* show the spectral characteristics at the sensors' drop ports, showing the result of the interaction of two spectra (the spectrum at the through port of the shaper and the drop port of the sensors) for the scheme of operation with the shaper MRR1 and MRR2, respectively, Fig. 10*c* and 10*d* show the registered power at the sensors' drop ports as the fluid RI changes. The average sensitivity and the coefficient D for the two schemes are: $S_{m1}=1430$ dB/RIU and $S_{m2}=186.67$ dB/RIU; $D_{m1}=1.01\cdot10^{-4}$ RIU and $D_{m2}=2.08\cdot10^{-4}$ RIU.

As one can see, the average sensitivity on through ports is much less than that on the drop ports in both cases. This is because, although the detected power level on the through ports is much higher, they have less contrast. This can be seen when comparing the spectra in Fig. 9 and 10. The contrast greatly influences the sensitivity of the sensing system as a whole, and its significance increases with the width of the analyzed spectrum range. Suppose one selects and analyzes only the range where the frequency response of the sensor changes depending on the frequency response of the shaper. In that case, the contrast will no longer be decisive, and the sensitivity at both ports will increase and become approximately the same.

Fig. 11 shows the simulation results for the relative power level calculated using equation (10). Calculated values of sensitivity and non-linearity coefficients are: $S_{m1}=1523.3$ dB/RIU; $S_{m2}=203.3$ dB/RIU; $D_{m1}=9.66\cdot10^{-5}$ RIU; $D_{m2}=2.03\cdot10^{-4}$ RIU.

4.2. Using the shaper's drop port as a signal source

The operation principle of the interrogating circuit with the drop port of the shaper MRR is mostly the same as the method described above, except that the shaping signal is fed from the shaper MRR's drop port. Fig. 12 – 14 show the operation results of all schemes' variations. For the scanning system detecting the output power on the sensors' through ports (Fig. 14, we achieved the following values of the

average sensitivity S_m and non-linearity coefficient D. For the shaper MRR1 (Fig. 12*a*, *c*), $S_{m1}=130$ dB/RIU, $D_{m1}=2.3\cdot10^{-4}$ RIU, while for the shaper MRR2 (Fig. 12*b*, *d*), $S_{m2}=90$ dB/RIU, $D_{m2}=8.2\cdot10^{-4}$ RIU. We achieved the following values for the scanning system detecting the output power on the sensors' drop ports (Fig. 9). For the shaper MRR1 (Fig. 13*a*, c), $S_{m1}=593.3$ dB/RIU, $D_{m1}=2.7\cdot10^{-4}$ RIU, while for the shaper MRR2 (Fig. 13*b*, *d*), $S_{m2}=1890$ dB/RIU, $D_{m2}=2.6\cdot10^{-5}$ RIU. Fig. 10 shows the dependence of the relative power level in the scanning circuit with the drop port of the shaper MRR on the change in the liquid RI and the corresponding linear approximation. Measuring the relative power, we achieved $S_{m1}=716.67$ dB/RIU, $D_{m1}=2.58\cdot10^{-4}$ RIU for the shaper MRR1, and $S_{m1}=1980$ dB/RIU, $D_{m1}=1.89\cdot10^{-5}$ RIU for the shaper MRR2.

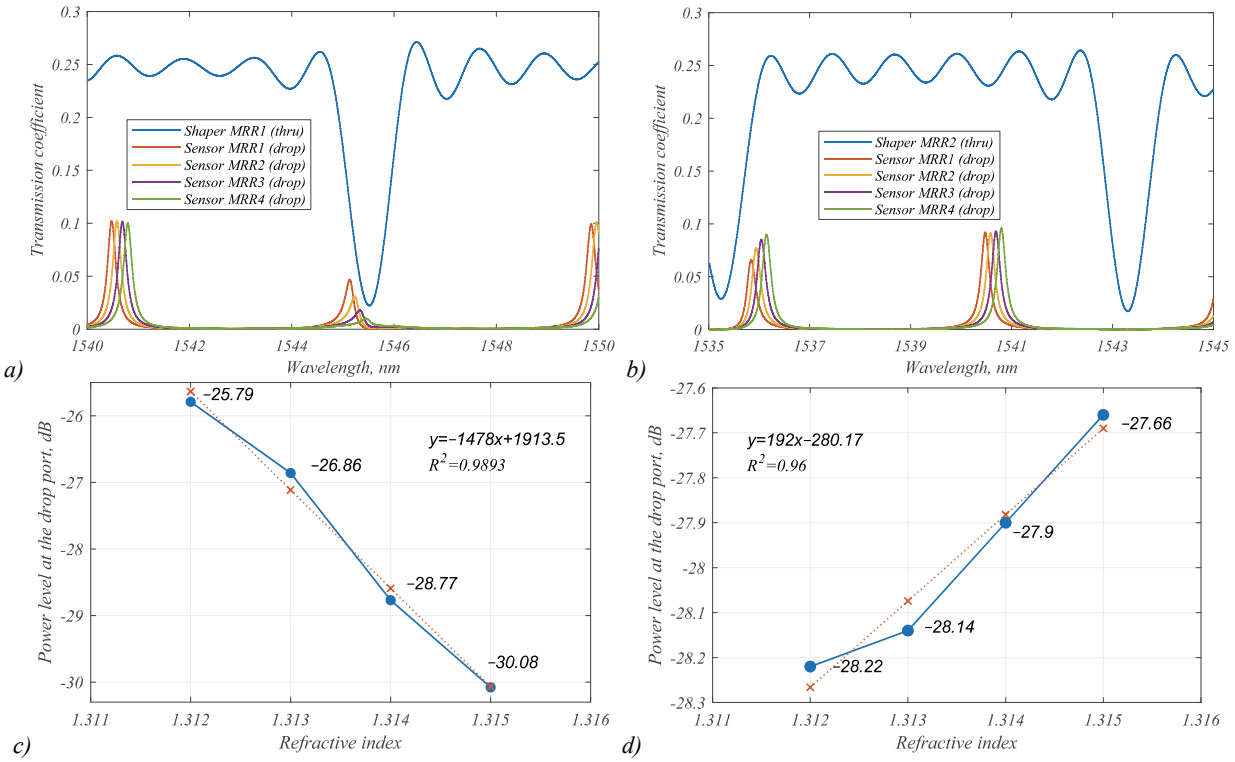

Fig. 10. Transmission spectra at the sensors' drop ports depending on the spectrum shape coming from the shaper MRR's through port for the scanning circuit with MRR1 (a), and for the scanning circuit with MRR2 (b); dependence of the received power on the sensors' through ports on the change in the liquid RI and its linear approximation (c) for the scanning circuit with MRR1, and (d) for the scanning circuit with MRR2

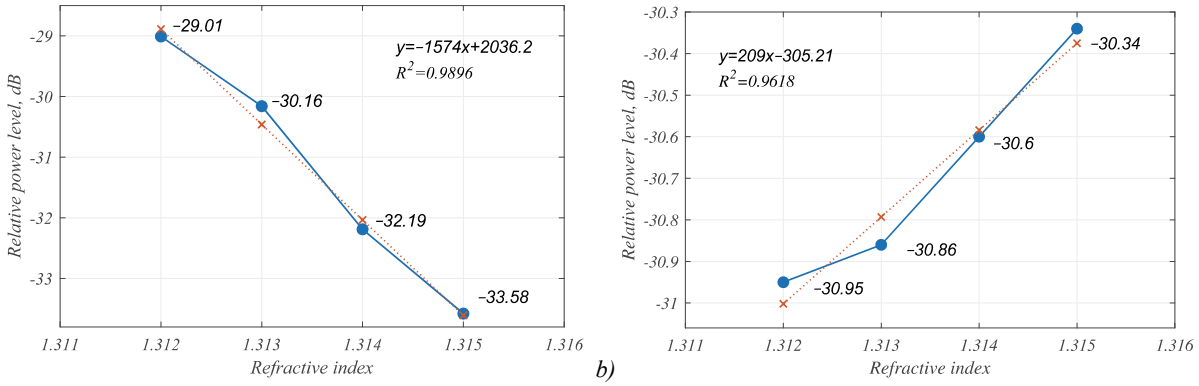

Fig. 11. Dependencies of the relative power level in the interrogating circuit from the shaper MRR's through port on the change in the liquid RI and its linear approximation for the interrogation circuit with MRR1 (a), and for the interrogation circuit with MRR2 (b)

4.3. Simulation results analysis

Tab. 2 shows all the results obtained for the average sensitivity and average D of all variations of the interrogating schemes. When comparing the results of the operation of the sensing system and the sensor separately ($S=110$ nm/RIU at $D=5.9\cdot10^{-4}$ RIU), one can see that the results of modeling the sensing system from a circuit with an MRR-based spectrum shaper often outperform the sensor itself. This allows us to conclude that the proposed method of simultaneous interrogation of a cascade of parallel-connected sensors increases the sensitivity of the sensing system to changes in the RI of the analyte. Also, when comparing the results, it can be noted that interrogation

using the sensors' drop ports gives the best result in the scheme with the shaper MRR with a racetrack section. Using the through port, the results are better for a MRR without a racetrack. When fixing the power at the outputs of the sensor ports separately, the sensitivity and the nonlinearity coefficient turned out to be much better than when using the shaper MRR's drop port in all circuit implementations. This is, as previously indicated, due to the contrast of the spectral characteristic. The best performance of a multi-channel sensing system is provided by calculating the relative power level using the shaper's drop port signal for interrogating the sensors.

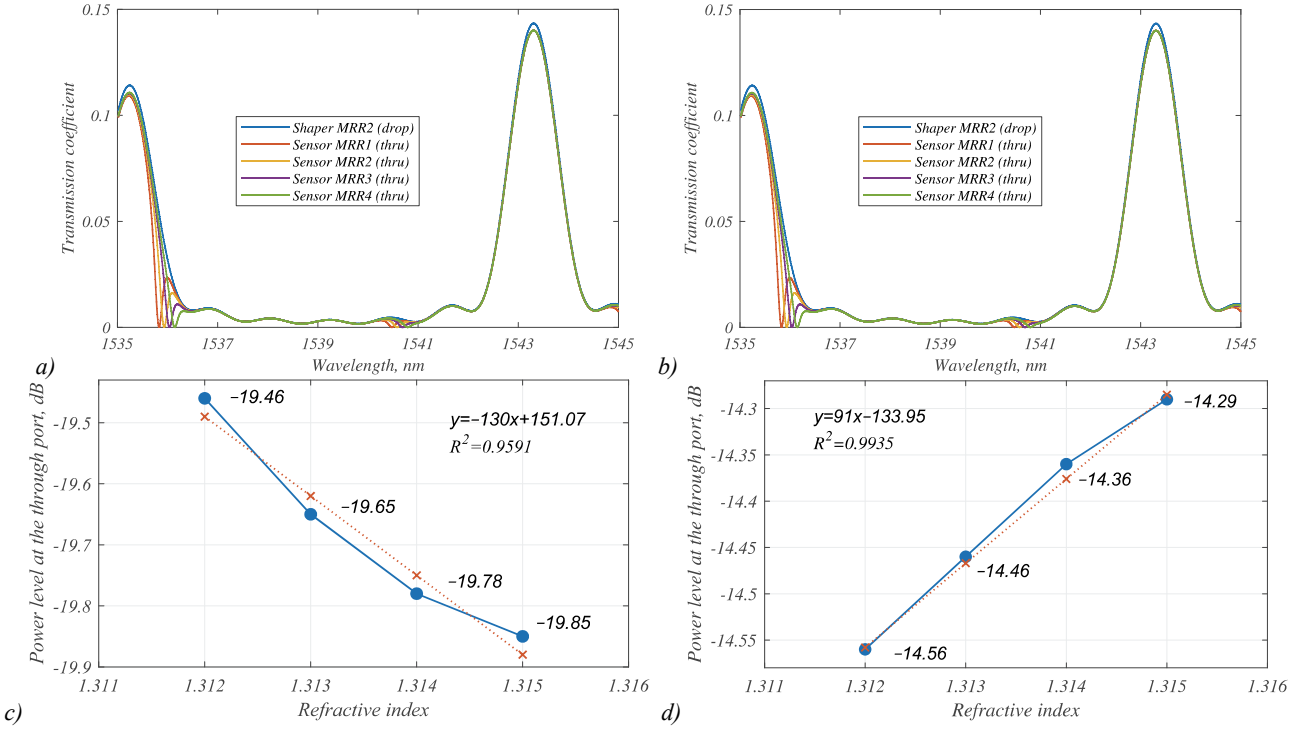

Fig. 12. Transmission spectra at the through ports of the sensor depending on the spectrum shape coming from the drop port of the shaper MRR for the scanning circuit with MRR1 (a) and for the scanning circuit with MRR2 (b); dependence of the received power on the through ports of the sensors on the change in the liquid RI and the linear approximation for the scanning system with the MRR1 (c) and the MRR2 (d)

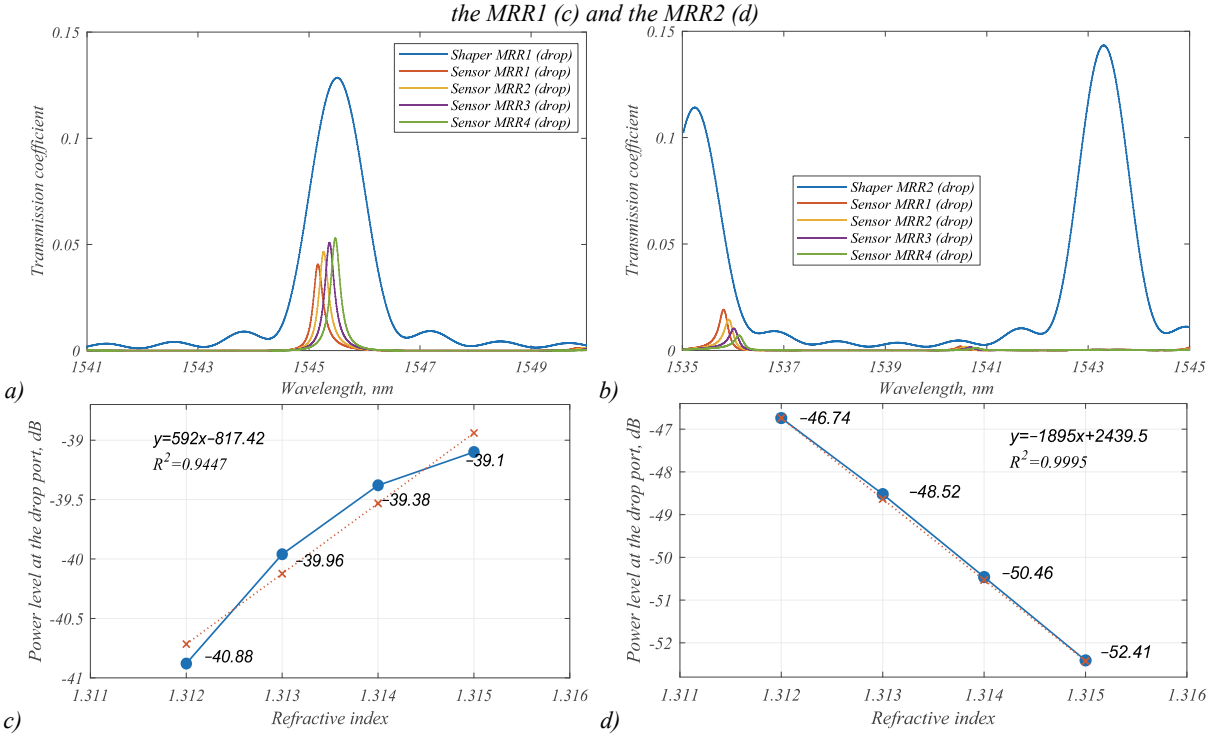

Fig. 13. Transmission spectra at the drop ports of the sensor depending on the spectrum shape coming from the drop port of the shaper MRR a) for the scanning circuit with MRR1, and b) for the scanning circuit with MRR2; dependence of the received power on the through ports of the sensors on the change in the liquid RI and the linear approximation for the scanning system with (c) the MRR1, and (d) the MRR2

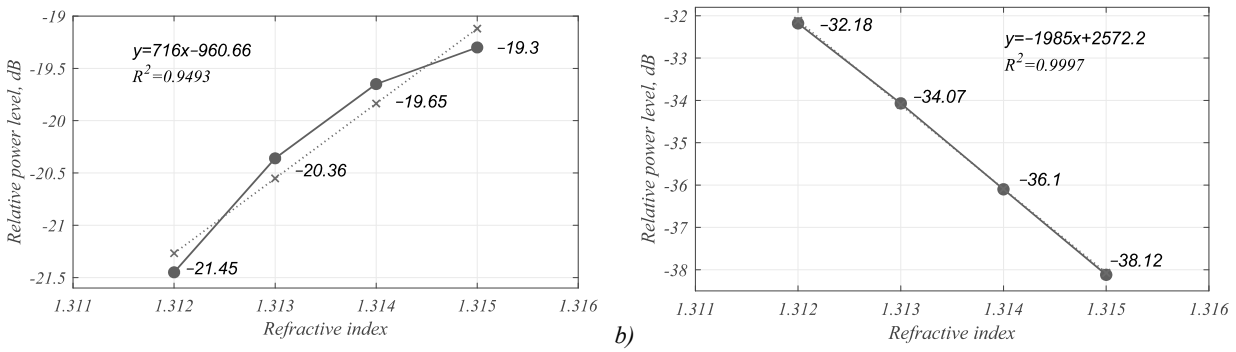

a) b)

Fig. 14. Dependencies of the relative power level in the interrogating circuit from the shaper MRR's through port of the on the change in the liquid RI and the linear approximation for the scanning system with the MRR1 (a), and the MRR2 (b)

Tab. 2. Simulation results for the tested scanning schemes

Racetrack MRR	Shaper port	S_m (measuring the relative power), dB/RIU	S_m thru/ drop, dB/RIU	D_m (measuring the relative power), RIU	D_m thru/ drop, RIU
+	thru	203.3	16.67/ 186.67	$2.03 \cdot 10^{-4}$	$1.47 \cdot 10^{-4}$/$2.08 \cdot 10^{-4}$
+	drop	1980	90/ 1890	$1.89 \cdot 10^{-5}$	$8.2 \cdot 10^{-5}$/$2.6 \cdot 10^{-5}$
–	thru	1523.3	93.3/ 1430	$9.66 \cdot 10^{-5}$	$1.13 \cdot 10^{-4}$/ $1.01 \cdot 10^{-4}$
–	drop	716.67	130/ 593.3	$2.58 \cdot 10^{-4}$	$2.3 \cdot 10^{-4}$ / $2.7 \cdot 10^{-4}$

Conclusion

We have proposed and analyzed a novel multichannel integrated photonic sensing system for liquid refractometry. Its distinguishing feature is the presence of a spectrum shaper that determines the signal level at the sensor's input port. This structure allows using one spectrum shaper to interrogate several sensors. We simulated the interrogation of four sensors. The results showed that the sensors' interrogation using the drop-port signal of the racetrack MRR-based shaper when registering the relative power at the sensors' output ports provides the best sensitivity. The best linearity is provided by interrogation using the drop-port signal of the MRR-based shaper when registering the relative power at the sensors' output ports. Based on the foregoing, thesuggested architecture may be useful for implementing fully integrated laboratory-on-a-chip optical structures and distributed sensing systems.

Acknowledgments

The research was supported by the Ministry of Science and Higher Education of the Russian Federation: state assignment for USATU, agreement № 075-03-2021-014 dated 29.09.2021 (FEUE-2021-0013).

References

[1] Li H, An Z, Mao Q, Zuo S, Zhu W, Zhang S, Zhang C, Li E, Garcia JDP. SOI waveguide bragg grating photonic sensor for human body temperature measurement based on photonic integrated interrogator, Nanomaterials 2021; 12(1): 29. DOI: 10.3390/nano12010029.

[2] Vogelbacher F, Kothe T, Muellner P, Melnik E, Sagmeister M, Kraft J, Hainberger R. Waveguide Mach-Zehnder biosensor with laser diode pumped integrated single-mode silicon nitride organic hybrid solid-state laser. Biosens Bioelectron 2022; 197: 113816. DOI: 10.1016/j.bios.2021.113816.

[3] Sun X, Dai D, Thylén L, Wosinski L. High-sensitivity liquid refractive-index sensor based on a Mach-Zehnder interferometer with a double-slot hybrid plasmonic waveguide. Opt Express 2015; 23(20): 25688-25699. DOI: 10.1364/OE.23.025688.

[4] Wu S, Guo Y, Wang W, Zhou J, Zhang Q. Label-free biosensing using a microring resonator integrated with poly-(dimethylsiloxane) microfluidic channels. Rev Sci Instrum 2019; 90: 035004. DOI: 10.1063/1.5074134.

[5] Guo C, Wang C, Ma T, Zhang L, Wang F. Integrated refractive index sensor based on an AlN-PSiO_2 hybrid plasmonic microdisk resonator. Appl Opt 2022; 61(17): 4980-4985. DOI: 10.1364/AO.458340.

[6] Butt MA, Khonina SN, Kazanskiy NL. A highly sensitive design of subwavelength grating double-slot waveguide microring resonator. Laser Phys Lett 2020; 17(7): 076201. DOI: 10.1088/1612-202X/ab8faa.

[7] Butt MA, Kazanskiy NL, Khonina SN. Modal characteristics of refractive index engineered hybrid plasmonic waveguide. IEEE Sens J 2020; 20(17): 9779-9786. DOI: 10.1109/JSEN.2020.2991215.

[8] Matsuura S, Yamasaku N, Nishijima Y, Okazaki S, Arakawa T. Characteristics of highly sensitive hydrogen sensor based on Pt-WO_3/Si microring resonator. Sensors 2019; 20(1): 96. DOI: 10.3390/s20010096.

[9] Wang J, Zhang X, Wei Z, Qiu H, Chen Y, Geng Y, Du Y, Cheng Z, Li X. Design of a dual-mode graphene-on-microring resonator for optical gas sensing. IEEE Access 2021; 9: 56479-56485. DOI: 10.1109/ACCESS.2021.3072134.

[10] Ma X, Chen K, Wu J, Wang L. Low-cost and highly sensitive liquid refractive index sensor based on polymer horizontal slot waveguide. Photonic Sens 2020; 10(1): 7-15. DOI: 10.1007/s13320-019-0560-y.

[11] Voronkov G, Zakoyan A, Ivanov V, Iraev D, Stepanov I, Yuldashev R, Grakhova E, Lyubopytov V, Morozov O, Kutluyarov R. Design and modeling of a fully integrated microring-based photonic sensing system for liquid refractometry. Sensors 2022; 22(23): 9553. DOI: 10.3390/s22239553.

[12] Tozzetti L, Bontempi F, Giacobbe A, Pasquale FD, Faralli S. Fast FBG interrogator on chip based on silicon on insulator ring resonator add/drop filters. J Lightw Technol 2022; 40(15): 5328-5336. DOI: 10.1109/JLT.2022.3174770.
[13] Yang F, Zhang W, Jiang Y, Tao J, He Z. Highly sensitive integrated photonic sensor and interrogator using cascaded silicon microring resonators. J Lightw Technol 2022; 40(9): 3055-3061. DOI: 10.1109/JLT.2022.3145501.
[14] Yang F, Zhang W, Zhao S, Liu Q, Tao J, He Z. Miniature interrogator for multiplexed FBG strain sensors based on a thermally tunable microring resonator array. Opt Express 2019; 27(5): 6037-6046. DOI: 10.1364/OE.27.006037.
[15] Liu Y, Li Y, Li M, He J-J. High-sensitivity and wide-range optical sensor based on three cascaded ring resonators. Opt Express 2017; 25(2): 972-978. DOI: 10.1364/OE.25.000972.
[16] Hoste J-W, Soetaert P, Bienstman P. Improving the detection limit of conformational analysis by utilizing a dual polarization Vernier cascade. Opt Express 2016; 24(1): 67-81. DOI: 10.1364/OE.24.000067.
[17] Weng S, Yuan P, Lu L, Zhang D, Zhu L. SOI-based arrayed waveguide grating with extended dynamic range for fiber Bragg grating interrogator. Opt Fiber Technol 2022; 68: 102815. DOI: 10.1016/j.yofte.2021.102815.
[18] Li K, Yuan P, Lu L, Dong M, Zhu L. PLC-based arrayed waveguide grating design for fiber Bragg grating interrogation system. Nanomaterials 2022; 12(17): 2938. DOI: 10.3390/nano12172938.
[19] Dai Y, Liu Y, Leng J, Deng G, Asundi A. A novel time-division multiplexing fiber Bragg grating sensor interrogator for structural health monitoring. Opt Lasers Eng 2009; 47(10): 1028-1033. DOI: 10.1016/j.optlaseng.2009.05.012.
[20] Hu C, Bai W. High-speed interrogation for large-scale fiber Bragg grating sensing. Sensors 2018; 18(3): 665. DOI: 10.3390/s18020665.
[21] Gotten M, Lochmann S, Ahrens A, Lindner E, Vlekken J, Van Roosbroeck J. A CDM-WDM interrogation scheme for massive serial FBG sensor networks. IEEE Sens J 2022; 22(12): 11290-11296. DOI: 10.1109/JSEN.2021.3070446.
[22] Rabus DG. Ring resonators: Theory and modeling. In Book: Rabus DG. Integrated ring resonators. Berlin, Heidelberg: Springer; 2007: 3-40. DOI: 10.1007/978-3-540-68788-7_2.
[23] Xia H, Wang C, Blais S, Yao J. Ultrafast and precise interrogation of fiber Bragg grating sensor based on wavelength-to-time mapping incorporating higher order dispersion. J Lightw Technol 2010; 28(3): 254-261. DOI: 10.1109/JLT.2009.2037722.
[24] Palik ED, Ghosh G. Handbook of optical constants of solids. San Diego: Academic Press; 1998.
[25] Lu Z, Jhoja J, Klein J, Wang X, Liu A, Flueckiger J, Pond J, Chrostowski L. Performance prediction for silicon photonics integrated circuits with layout-dependent correlated manufacturing variability. Opt Express 2017; 25(9): 9712-9733. DOI: 10.1364/OE.25.009712.
[26] Chrostowski L, Hochberg M. Silicon photonics design: From devices to systems. 1st ed. Cambridge: Cambridge University Press; 2015. ISBN: 978-1-107-08545-9.
[27] Bogaerts W, De Heyn P, Van Vaerenbergh T, De Vos K, Kumar Selvaraja S, Claes T, Dumon P, Bienstman P, Van Thourhout D, Baets R. Silicon microring resonators. Laser Photon Rev 2012; 6(1): 47-73.
[28] Milvich J, Kohler D, Freude W, Koos C. Integrated phase-sensitive photonic sensors: a system design tutorial. Adv Opt Photon 2021; 13(3): 584-642. DOI: 10.1364/AOP.413399.
[29] Wang X, Flueckiger J, Schmidt S, Grist S, Fard ST, Kirk J, Doerfler M, Cheung KC, Ratner DM, Chrostowski L. A silicon photonic biosensor using phase-shifted Bragg gratings in slot waveguide. J Biophotonics 2013; 6(10): 821-828. DOI: 10.1002/jbio.201300012.

Authors' information

Aida Gaykovna Zakoyan, (b. 2000) graduated with honors (2021) from Ufa State Aviation Technical University (USATU), majoring in Infocommunication Technologies and Communication Systems. Currently she is a graduate student at the Ufa University of Science and Technology and works at the research laboratory "Sensor systems based on integrated photonics devices". Her research interests are: integrated photonics, spectroscopy in astronomy, satellite communications. E-mail: *zakoyan.ag@ugatu.su*

Grigory Sergeevich Voronkov (b. 1986) graduated with honors (2007) from Ufa State Aviation Technical University (USATU), majoring in Communications with Mobile Devices. He has defended Candidate of Sciences thesis in 2017. Currently he works as an assistant professor and a senior researcher at the Ufa University of Science and Technology, research laboratory "Sensor systems based on integrated photonics devices". His current research interests include signal processing, microwave systems, integrated photonics. E-mail: *voronkov.gs@ugatu.su*

Vladimir Sergeevich Lyubopytov (b. 1986) graduated with honors (2008) from Ufa State Aviation Technical University (USATU), majoring in Multichannel Telecommunication Systems. He has defended the Candidate of Sciences thesis in 2013. Currently he works as a senior researcher at the research laboratory "Sensor systems based on integrated photonics devices", Ufa University of Science and Technology. His current research interests include integrated photonics, high-speed optical communications, microwave photonics, optical computing.
E-mail: *lyubopytov.vs@ugatu.su*

Albert Khanovich Sultanov (b. 1950) graduated with honors (1973) from the Novosibirsk Electrotechnical Institute of Telecommunications (at present the Siberia State University of Telecommunications and Informatics), majoring in Multichannel Electrocommunications. He received his Doctor in Technical Sciences degree (1996) from Ufa State Aviation Technical University (USATU). Currently he is a Professor at the Telecommunication Systems

department, Ufa University of Science and Technology. He is a SPIE member, Academic of the Telecommunication Academy. His current research interests include telecommunications, fiber optics, integrated photonics, aerospace systems, microsatellite communications. E-mail: *tks@ugatu.su*

Elizaveta Pavlovna Grakhova (b. 1990) graduated with honors (2012) from Ufa State Aviation Technical University, majoring in Radiocommunications, Radiobroadcasting and Television. She has defended the Candidate of Sciences thesis in 2016. Currently she is the Head of the research laboratory "Sensor systems based on integrated photonics devices" at the Ufa University of Science and Technology. Her current research interests include signal processing, antenna technology, microwave photonics. E-mail: *grakhova.ep@ugatu.su*

Ruslan Vladimirovich Kutluyarov (b. 1986) graduated with honors (2008) from Ufa State Aviation Technical University (USATU), majoring in Multichannel Telecommunication Systems. He has defended the Candidate of Sciences thesis in 2013. Currently he works as a senior researcher at the research laboratory "Sensor systems based on integrated photonics devices" and an assistant professor at the Telecommunication Systems department, Ufa University of Science and Technology. His current research interests include integrated photonics, nonlinear optics, fiber optics, microwave photonics, quantum communications. E-mail: *kutluyarov.rv@ugatu.su*

Received December 29, 2022. The final version – May 4, 2023.